


Depleted Higgs boson: Searches for universal coupling suppression, invisible decays, and mixed-in scalars

Prudhvi N. Bhattiprolu  and James D. Wells

Leinweber Center for Theoretical Physics, University of Michigan, Ann Arbor, Michigan 48109, USA

 (Received 1 November 2022; accepted 21 February 2023; published 14 March 2023)

Two simple ways by which the standard signals of the Standard Model Higgs boson can be depleted are its couplings to fermions and gauge bosons can be suppressed by a universal factor, and part of its branching fraction can be drained into invisible final states. A large class of theories can impose one or both of these depletion factors, even if mild, by way of additional scalar bosons that are singlets under the Standard Model but mix with the Higgs boson. We perform a comprehensive survey of the present status of the depleted Higgs boson, and discuss future prospects for detecting the presence of either depletion factor. We also survey the constraints status and future detection prospects for the generic case of extra mixed-in scalars which generically lead to these depletion factors for the Higgs boson. We find, for example, that precision study of the Higgs boson in many cases is more powerful than searches for the extra scalar states, given the slate of next-generation experiments that are on the horizon.

DOI: [10.1103/PhysRevD.107.055022](https://doi.org/10.1103/PhysRevD.107.055022)

I. INTRODUCTION

One of the biggest triumphs of the Standard Model (SM) is the explanation of the electroweak symmetry breaking via a CP -even complex scalar $H \sim (\mathbf{1}, \mathbf{2}, \frac{1}{2})$, which further predicts the existence of a neutral Higgs boson h_{SM} that is part of the neutral component of the $SU(2)_L$ doublet H . So far all the measured properties of the ~ 125 GeV physical Higgs boson that was discovered in 2012 at the Large Hadron Collider (LHC) are consistent with the SM predictions and therefore the observed Higgs boson h is often identified as the SM Higgs boson h_{SM} .

It is important to note, however, that as the Higgs measurements get more precise there is a well-motivated possibility that the observations can deviate from the SM predictions thereby pointing towards the presence of a more complicated Higgs sector. In this paper we study the prospect of the observed Higgs boson h having a universal depletion factor δ , suppressing all its couplings to the SM states, along with an invisible width.¹ The invisible width constitutes a second depletion factor for the Higgs boson because its standard decay final state branching fractions are depleted due to the additional invisible mode.

¹See also Refs. [1,2] for related studies on the impact of two universal depletion factors on Higgs signal strength measurements.

Published by the American Physical Society under the terms of the Creative Commons Attribution 4.0 International license. Further distribution of this work must maintain attribution to the author(s) and the published article's title, journal citation, and DOI. Funded by SCOAP³.

To set notation, the SM Higgs boson h_{SM} is related to the observed Higgs boson h in the following way:

$$h_{\text{SM}} = \sqrt{1 - \delta^2} h + \dots, \quad (1.1)$$

where \dots include contributions from additional physical Higgs states that can arise from extended Higgs sectors. In other words, we identify the label ‘‘Higgs boson’’ h with the h_{125} discovered resonance and not necessarily with the platonic ideal Standard Model Higgs boson h_{SM} . Below, we obtain constraints on the universal depletion factor δ , dependent on the invisible width of h , from various searches for the ~ 125 GeV Higgs boson at the LHC while remaining agnostic to the particulars of the extended Higgs sectors. We also later reinterpret some projections at the International Linear Collider (ILC) and the High Luminosity LHC (HL-LHC) from the invisible decays of h . We emphasize that the relation in Eq. (1.1) can naturally arise from many extended Higgs sectors.

As a concrete example for an extended Higgs sector that leads to a universal depletion factor δ and an invisible width for h , we first consider an extension to the SM with a real scalar $S \sim (\mathbf{1}, \mathbf{1}, 0)$ that mixes with the SM Higgs boson h_{SM} to give rise to two physical mass eigenstates: the observed Higgs h and an exotic Higgs ϕ . We take the singlet scalar S to only have invisible decays which translates to an invisible width for h via its mixing with S . SM extensions with a singlet scalar were extensively studied in the literature; see, e.g., Refs. [3–23] and references therein.

For illustration purposes, we only restrict ourselves to the mass of the exotic Higgs ϕ to be in between $m_h/2$ and $2m_h$

such that the decays $h \rightarrow \phi\phi$ and $\phi \rightarrow hh$ are kinematically forbidden. We will see below that after reexamining the parameter space with the latest bounds, the indirect constraints from the precision probes for the observed Higgs boson h at the LHC are the dominant ones in general compared to the bounds from the searches for additional neutral Higgs states, and from the oblique parameters S , T , and U . This is in accord with the findings in Refs. [16,17] for $m_h/2 \leq m_\phi \leq 2m_h$ specifically for the case where h does not have any invisible decays.

We also show some future projections at the ILC. As a further extension to this case, we also briefly consider the case with N such scalars that are assumed to mix equally among themselves, and with the SM Higgs boson. Once again, as we will see below, we find the indirect bounds from precision probes for the observed Higgs boson h moderately constrain the parameter space, which gets stronger as N and/or the invisible width of h gets larger.

The remaining sections of this paper are structured as follows. In Sec. II, we define “the depleted Higgs boson”—Higgs boson with a universal suppression and invisible width—and obtain its production cross sections, total width, and branching ratios relative to that of the 125 GeV Higgs in the SM. In Sec. III we study the constraints on the universal depletion factor δ , which varies with the invisible width of h , from the latest LHC precision probes for the ~ 125 GeV Higgs boson in various decay channels. We also consider some example future projections from ILC and HL-LHC. In Sec. IV, we consider the SM extension with a real singlet scalar, and in Sec. V we reexamine the present direct and indirect bounds along with some future projections from collider searches, and the current constraints from the Peskin-Takeuchi S , T , and U parameters. We also briefly consider a Higgs sector with N real singlet scalars, under some simplifying assumptions, and study the implications of direct and indirect searches on such a scenario in Sec. VI. Finally, we end with some concluding remarks in Sec. VII.

II. HIGGS BOSON WITH A UNIVERSAL SUPPRESSION AND INVISIBLE WIDTH

Consider the Higgs boson h with its mass of ~ 125 GeV and with a universal depletion factor δ for all its couplings to the SM states, such that the production cross sections of h are given by

$$\sigma^h = (1 - \delta^2)\sigma_{\text{SM}}^{125}, \quad (2.1)$$

where σ_{SM}^{125} are the production cross sections for 125 GeV Higgs in the SM. Additionally, assume that the 125 GeV Higgs also has an invisible width that is parametrized as $\delta^2\Gamma_{\text{inv}}$. Therefore, the total width of h is

$$\Gamma^h = (1 - \delta^2)\Gamma_{\text{SM}}^{125} + \delta^2\Gamma_{\text{inv}}, \quad (2.2)$$

where Γ_{SM}^{125} stands for the total width of the 125 GeV Higgs boson in the SM. Upon defining

$$\kappa_{\text{inv}} \equiv \Gamma_{\text{inv}}/\Gamma_{\text{SM}}^{125}, \quad (2.3)$$

Equation (2.2) can be reexpressed as

$$\frac{\Gamma^h}{\Gamma_{\text{SM}}^{125}} = 1 - (1 - \kappa_{\text{inv}})\delta^2. \quad (2.4)$$

Given these definitions, the ratio of the branching ratio B_j^h of $h \rightarrow j^{\text{th}}$ SM final state to that of the corresponding branching ratio in the SM $B_{\text{SM},j}^{125}$, and the invisible branching ratio B_{inv}^h can be entirely expressed in terms of just two parameters $-\delta$ and κ_{inv} :

$$\frac{B_j^h}{B_{\text{SM},j}^{125}} = \frac{1 - \delta^2}{1 - (1 - \kappa_{\text{inv}})\delta^2}, \quad (2.5)$$

$$B_{\text{inv}}^h = \frac{\delta^2\kappa_{\text{inv}}}{1 - (1 - \kappa_{\text{inv}})\delta^2}. \quad (2.6)$$

Note that in the limit $\delta \rightarrow 0$ the SM is completely recovered (independent of κ_{inv} or Γ_{inv}).

Although, at this point, the appearance of the terms δ and Γ_{inv} (or, equivalently, κ_{inv}) might seem *ad hoc*, we later consider the case where the SM is extended by a real scalar $S \sim (\mathbf{1}, \mathbf{1}, 0)$ that decays invisibly and mixes with the SM Higgs boson h_{SM} . In which case, δ will be the sine of the mixing angle between h_{SM} and S , and Γ_{inv} is the invisible decay width of S . More generally, the terms δ and κ_{inv} naturally appear in many models beyond the SM, since these “singlets” can represent any number of possible states with exotic charges in a sector beyond the SM. Furthermore, we will see that the constraints on δ and κ_{inv} that come just from the precision probes for the 125 GeV SM Higgs boson moderately constrain the extensions to the Higgs sector. The case with $N \geq 1$ real singlet Higgs boson(s) that we later consider will illustrate that.

III. CONSTRAINTS ON DEPLETION FACTORS δ AND κ_{inv}

We now turn to constraints on the two-dimensional parameter space of $(\delta, \kappa_{\text{inv}})$ that come from searches by ATLAS and CMS Collaborations at the LHC for the observed Higgs boson decaying invisibly or to the SM final states. From invisible searches, a bound is usually reported on the invisible branching ratio B_{inv} of the Higgs boson multiplied with its production cross section relative to the production cross section in the SM $\sigma/\sigma_{\text{SM}}$. In particular, an upper bound is reported on μ_{inv}^2 which we define as

TABLE I. Recent LHC searches for invisible decays of the 125 GeV Higgs boson by ATLAS and CMS experiments along with the reported 95% C.L. upper bounds on μ_{inv} . μ_{inv} is defined to be the product of the invisible branching fraction of the Higgs boson and its production cross section relative to that of the SM. For convenience, various searches are assigned labels which will be used in the figure(s).

Label	95% C.L. upper bound on μ_{inv}	References
ATLAS 2020 ($h \rightarrow \text{inv}$)	0.11	[24]
ATLAS 2020 ($h \rightarrow \text{inv}$, 13 TeV)	0.13	[24]
CMS 2018 ($h \rightarrow \text{inv}$)	0.18	[25]
CMS 2018 ($h \rightarrow \text{inv}$, 13 TeV)	0.33	[25]

$$\mu_{\text{inv}} \equiv \frac{\sigma}{\sigma_{\text{SM}}} B_{\text{inv}}, \quad (3.1)$$

which in our case can be written as [see Eq. (2.1)]

$$\mu_{\text{inv}} = (1 - \delta^2) B_{\text{inv}}^h. \quad (3.2)$$

Therefore, using Eq. (2.6), the above equation imposes the following constraint on $(\delta, \kappa_{\text{inv}})$ parameter space

$$\frac{\delta^2(1 - \delta^2)\kappa_{\text{inv}}}{1 - (1 - \kappa_{\text{inv}})\delta^2} < \mu_{\text{inv}}. \quad (3.3)$$

Table I shows some recent LHC upper bounds on the quantity μ_{inv} at 95% C.L. by ATLAS and CMS experiments.

As for visible final states, precision probes for the decay of the 125 GeV Higgs boson to a j th SM final state often report the measured signal strength modifier μ defined as

$$\mu_{-\sigma_{\mu}^{-}}^{+\sigma_{\mu}^{+}} = \frac{\sigma B_j}{\sigma_{\text{SM}} B_{\text{SM},j}}, \quad (3.4)$$

where $+\sigma_{\mu}^{+}$, $-\sigma_{\mu}^{-}$ account for various systematic and statistical uncertainties on μ . In our case, the above equation also provides a constraint on $(\delta, \kappa_{\text{inv}})$ parameter space [see Eqs. (2.1) and (2.5)], which we obtain by solving for δ as a function a κ_{inv} (or vice versa) from

$$\chi^2 = \frac{1}{\sigma_{\mu}^2} \left(\mu - \frac{(1 - \delta^2)^2}{1 - (1 - \kappa_{\text{inv}})\delta^2} \right)^2. \quad (3.5)$$

Here, we require $\chi^2 = 5.99$ which corresponds to a fit with 95% confidence level with 2 degrees of freedom [26], and we simply take $\sigma_{\mu} = (\sigma_{\mu}^{+} + \sigma_{\mu}^{-})/2$ [as we will be concerned

²For convenience, we define the invisible branching ratio of the Higgs boson multiplied with its production cross section relative to the production cross section in the SM as μ_{inv} , which is not to be confused with the signal strength modifier that is defined in Eq. (3.4).

TABLE II. Recent LHC precision probes for the 125 GeV Higgs boson decaying into the (visible) SM final states by ATLAS and CMS experiments along with the measured signal strength modifier μ and its overall uncertainty as reported by ATLAS/CMS that accounts for various systematic and statistical uncertainties. For convenience, various searches are assigned labels which will be used in the figure(s).

Label	Observed μ	References
CMS 2021 ($h \rightarrow \gamma\gamma$)	1.12 ± 0.09	[27]
ATLAS 2022 ($h \rightarrow \gamma\gamma$)	$1.04_{-0.09}^{+0.10}$	[28]
ATLAS 2020 ($h \rightarrow ZZ \rightarrow 4\ell$)	1.01 ± 0.11	[29]
CMS 2021 ($h \rightarrow ZZ \rightarrow 4\ell$)	0.94 ± 0.11	[30]
ATLAS 2022 ($h \rightarrow WW \rightarrow e\nu\mu\nu$)	1.09 ± 0.11	[31]
CMS 2020 ($h \rightarrow WW \rightarrow e\nu\mu\nu$)	1.05 ± 0.12	[32]
CMS 2018 ($h \rightarrow bb$)	1.04 ± 0.20	[33]
ATLAS 2018 ($h \rightarrow bb$)	1.01 ± 0.20	[34]
ATLAS 2022 ($h \rightarrow \tau\tau$)	$0.93_{-0.12}^{+0.13}$	[35]
CMS 2022 ($h \rightarrow \tau\tau$)	0.82 ± 0.11	[36]
CMS 2020 ($h \rightarrow \mu\mu$)	$1.19_{-0.42}^{+0.44}$	[37]
ATLAS 2020 ($h \rightarrow \mu\mu$)	1.2 ± 0.6	[38]

here with the cases where the asymmetry, $(\sigma_{\mu}^{+} - \sigma_{\mu}^{-})/(\sigma_{\mu}^{+} + \sigma_{\mu}^{-})$, is either small or absent]. Table II lists the observed μ from the recent LHC searches by ATLAS and CMS experiments for the decays of the 125 GeV Higgs boson to various SM final states.

Figure 1 shows the most recent bounds from the LHC precision probes for the 125 GeV Higgs boson h in various decay channels at 95% C.L. In each decay channel of h , only the strongest bound is shown in the figure. The shaded regions with dashed and solid borders show the bounds obtained from the searches for h to invisible and SM final states (excluding $h \rightarrow \gamma\gamma$), respectively. The bound obtained from the search for $h \rightarrow \gamma\gamma$ is shown by a dotted line. Here, a dotted line is used to emphasize that the $h \rightarrow \gamma\gamma$ is a loop-induced process, and is therefore more sensitive to new physics contributions.

The future searches, see, e.g., Refs. [39–46], for h further constrain this parameter space, and as candidate projections, we show the dash-dotted lines corresponding to the 95% C.L. expected sensitivity for the invisible decays of h at the high luminosity LHC (HL-LHC) with 3 ab^{-1} of integrated luminosity [40] and at the International Linear Collider (ILC) with silicon detector at $\sqrt{s} = 250 \text{ GeV}$ with an integrated luminosity of $(0.9, 0.9) \text{ ab}^{-1}$ for $(e_{L}^{-} e_{R}^{+}, e_{R}^{-} e_{L}^{+})$, respectively, and beam polarization of $(80, 30)\%$ for (e^{-}, e^{+}) , respectively [46].

Therefore, if the 125 GeV Higgs boson has a universal suppression for all its couplings to SM fermions and gauge bosons along with an invisible width, it is evident from Fig. 1 that this scenario is moderately constrained from the current LHC searches. And, the future precision studies of the already discovered Higgs boson should be able to further constrain or find evidence for such a scenario with

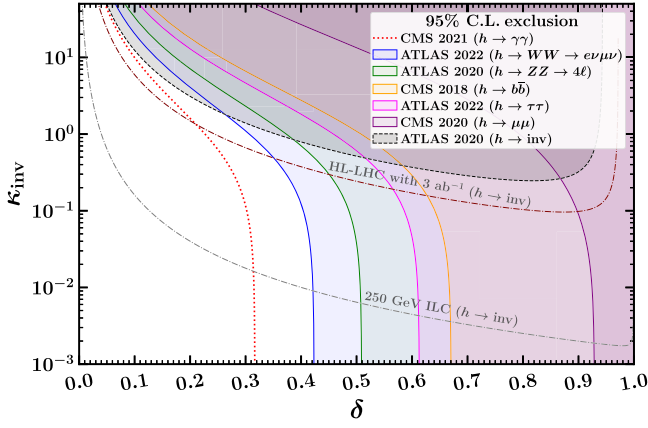


FIG. 1. Current 95% C.L. bounds on the parameter space of $(\delta, \kappa_{\text{inv}})$ from ATLAS and CMS precision probes for 125 GeV Higgs boson in various search channels. Out of the bounds obtained from the reported values of μ_{inv} [defined in Eq. (3.1)] and the signal strength modifier μ from Tables I and II, respectively, only the strongest bounds in each search channel are shown here. The shaded regions with dashed and solid borders show the bounds obtained from the searches for h to invisible and SM final states (excluding $h \rightarrow \gamma\gamma$), respectively. The bound from $h \rightarrow \gamma\gamma$ is shown by a dotted line to emphasize that the process is loop induced and therefore more sensitive to new physics contributions. The dash-dotted lines show the projected 95% C.L. sensitivity for invisible h decays at 250 GeV ILC and high luminosity LHC with nominal running assumptions as discussed in the text.

depletion factors $(\delta, \kappa_{\text{inv}})$. Thus the precision probes for the 125 GeV Higgs boson provide for an indirect, and often the most powerful probe (as we will see below for a few examples), for a large class of theories with depletion factors $(\delta, \kappa_{\text{inv}})$ for the 125 GeV Higgs and additional physical Higgs states.

IV. REAL SINGLET SCALARS EXTENSION

We now consider a model with the SM particle content and an additional real scalar Higgs S that is a singlet under the SM gauge group with the following scalar potential³:

$$V(H, S) = -m_H^2 H^\dagger H + \lambda(H^\dagger H)^2 + \frac{1}{2}m_S^2 S^2 + \mu_S H^\dagger HS, \quad (4.1)$$

where H is the SM Higgs doublet with a weak hypercharge $Y = 1/2$, and m_H^2 is positive such that H acquires a nonzero vacuum expectation value (VEV). The singlet Higgs S is assumed to have invisible decays, governed by the interaction Lagrangian

³We treat Eq. (4.1) as an effective scalar potential and therefore the tadpole term for S that naively seems to follow from Eq. (4.1) does not exist in the full theory (see, e.g., Refs. [3,4]).

$$\mathcal{L}_{\text{int}} = \lambda_\psi S \bar{\psi} \psi, \quad (4.2)$$

where $\psi \sim (\mathbf{1}, \mathbf{1}, 0)$ is a very light hidden-sector fermion with a Dirac mass m_ψ . Therefore, the width for S to decay to the invisible states $S \rightarrow \psi \bar{\psi}$ is $\Gamma_{\text{inv}}(m_S) \simeq \lambda_\psi^2 m_S / 8\pi$, with the assumption that $m_\psi \ll m_S$.

At the minimum of the scalar potential, we assume $\langle S \rangle = 0$, and we use $SU(2)_L$ gauge freedom such that only the neutral component H^0 of the SM Higgs doublet acquires a VEV. In unitary gauge, we take

$$\langle H^0 \rangle = \frac{v + h_{\text{SM}}}{\sqrt{2}}, \quad (4.3)$$

with $v = m_H / \sqrt{\lambda} (\simeq 246 \text{ GeV})$. After plugging in for H and expanding around the VEV, Eq. (4.1) becomes

$$V(h_{\text{SM}}, S) \supset \frac{1}{2} \begin{pmatrix} h_{\text{SM}} & S \end{pmatrix} \mathcal{M}^2 \begin{pmatrix} h_{\text{SM}} \\ S \end{pmatrix}, \quad (4.4)$$

with

$$\mathcal{M}^2 = \begin{pmatrix} 2m_H^2 & \mu_S v \\ \mu_S v & m_S^2 \end{pmatrix}. \quad (4.5)$$

The squared mass matrix can then be diagonalized by a unitary matrix parametrized by a mixing angle

$$\omega = \frac{1}{2} \tan^{-1} \frac{2\mu_S v}{m_S^2 - 2m_H^2}, \quad (4.6)$$

which leads to the physical mass eigenstates h, ϕ that are admixtures of the gauge eigenstates h_{SM}, S :

$$h_{\text{SM}} = \cos \omega h + \sin \omega \phi, \quad (4.7)$$

$$S = -\sin \omega h + \cos \omega \phi, \quad (4.8)$$

with their corresponding squared masses

$$m_\pm^2 = \frac{1}{2} \left[(m_S^2 + 2m_H^2) \pm \sqrt{(m_S^2 - 2m_H^2)^2 + 4\mu_S^2 v^2} \right], \quad (4.9)$$

where m_+ is the mass of the heavier state and m_- is the mass of the lighter state. We take h to be the physical Higgs boson h with mass $m_h \simeq 125 \text{ GeV}$ that was discovered at the LHC in 2012, and the other mass eigenstate ϕ to be the exotic Higgs. From Eqs. (4.6) to (4.9), note that as μ_S in Eq. (4.1) is tuned down to 0, the mixing angle ω vanishes and the mass eigenstates are the same as the gauge eigenstates with masses $2m_H^2 (\simeq 125 \text{ GeV})$ and m_S^2 . For purposes of illustration, in this paper, we only consider the possibility of having m_ϕ in the vicinity of

m_h , specifically $m_h/2 < m_\phi < 2m_h$, so that the decays $h \rightarrow \phi\phi$ and $\phi \rightarrow hh$ are kinematically forbidden.

Due to the mixing of the gauge eigenstates h_{SM} and S , the physical states h, ϕ can now decay to SM states and to invisible states with widths $\Gamma_{\text{SM}}^{h,\phi}$ and $\Gamma_{\text{inv}}^{h,\phi}$, respectively. Apart from the masses m_\pm (of which one is already known to be ~ 125 GeV), the widths, the production cross sections and branching fractions of h, ϕ can be expressed in terms of only two free parameters δ and κ_{inv} that are defined as

$$\delta \equiv |\sin \omega|, \quad (4.10)$$

$$\kappa_{\text{inv}} \equiv \Gamma_{\text{inv}}/\Gamma_{\text{SM}}^{125}. \quad (4.11)$$

In terms of Γ_{SM} (total width for h_{SM} to SM states) and Γ_{inv} (width for $S \rightarrow \psi\bar{\psi}$):

$$\Gamma_{\text{SM}}^\phi = \delta^2 \Gamma_{\text{SM}}(m_\phi), \quad \Gamma_{\text{inv}}^\phi = (1 - \delta^2) \Gamma_{\text{inv}}, \quad (4.12)$$

$$\Gamma_{\text{SM}}^h = (1 - \delta^2) \Gamma_{\text{SM}}^{125}, \quad \Gamma_{\text{inv}}^h = \delta^2 \Gamma_{\text{inv}}, \quad (4.13)$$

where Γ_{inv} is treated as a free parameter, and $\Gamma_{\text{SM}}^{125} = \Gamma_{\text{SM}}$ (125 GeV). Also, in terms of the production cross section σ_{SM} of h_{SM} , the production cross sections for h, ϕ are

$$\sigma^\phi = \delta^2 \sigma_{\text{SM}}(m_\phi), \quad (4.14)$$

$$\sigma^h = (1 - \delta^2) \sigma_{\text{SM}}^{125}. \quad (4.15)$$

We can now compare the production cross sections times branching ratios of h, ϕ to the ones in the SM. In order to do so, we first note that the total widths $\Gamma^{h,\phi}$ of h, ϕ are related to the SM width Γ_{SM} via

$$\frac{\Gamma^\phi}{\Gamma_{\text{SM}}} = \frac{\kappa_{\text{inv}} + (\kappa_{\text{SM}} - \kappa_{\text{inv}})\delta^2}{\kappa_{\text{SM}}}, \quad (4.16)$$

$$\frac{\Gamma^h}{\Gamma_{\text{SM}}^{125}} = 1 - (1 - \kappa_{\text{inv}})\delta^2, \quad (4.17)$$

where we have defined

$$\kappa_{\text{SM}} \equiv \Gamma_{\text{SM}}(m_\phi)/\Gamma_{\text{SM}}^{125}. \quad (4.18)$$

Using these results and definitions, the ratio of branching ratios of h, ϕ into the j th SM final state $B_j^{h,\phi} = \Gamma_j^{h,\phi}/\Gamma^{h,\phi}$ to that of the SM $B_{\text{SM},j}$ can be expressed as

$$\frac{B_j^\phi}{B_{\text{SM},j}} = \frac{\delta^2 \kappa_{\text{SM}}}{\kappa_{\text{inv}} + (\kappa_{\text{SM}} - \kappa_{\text{inv}})\delta^2}, \quad (4.19)$$

$$\frac{B_j^h}{B_{\text{SM},j}^{125}} = \frac{1 - \delta^2}{1 - (1 - \kappa_{\text{inv}})\delta^2}, \quad (4.20)$$

so the production rates of h, ϕ in the j th SM final state is

$$\frac{\sigma^\phi B_j^\phi}{\sigma_{\text{SM}} B_{\text{SM},j}} = \frac{\delta^4 \kappa_{\text{SM}}}{\kappa_{\text{inv}} + (\kappa_{\text{SM}} - \kappa_{\text{inv}})\delta^2}, \quad (4.21)$$

$$\frac{\sigma^h B_j^h}{\sigma_{\text{SM}}^{125} B_{\text{SM},j}^{125}} = \frac{(1 - \delta^2)^2}{1 - (1 - \kappa_{\text{inv}})\delta^2}. \quad (4.22)$$

Finally, the invisible branching ratios $B_{\text{inv}}^{h,\phi} = \Gamma_{\text{inv}}^{h,\phi}/\Gamma^{h,\phi}$ of h, ϕ :

$$B_{\text{inv}}^\phi = \frac{(1 - \delta^2)\kappa_{\text{inv}}}{\kappa_{\text{inv}} + (\kappa_{\text{SM}} - \kappa_{\text{inv}})\delta^2}, \quad (4.23)$$

$$B_{\text{inv}}^h = \frac{\delta^2 \kappa_{\text{inv}}}{1 - (1 - \kappa_{\text{inv}})\delta^2}. \quad (4.24)$$

Note that the expressions for h in Eqs. (4.15), (4.17), (4.20), and (4.24) match with Eqs. (2.1), (2.4)–(2.6), respectively.

Using the above equations, we can now obtain the current constraints/future sensitivities for real singlet scalar extension to the SM that impose the depletion factors $(\delta, \kappa_{\text{inv}})$ on the 125 GeV Higgs boson h and also predict an exotic Higgs ϕ . The indirect constraints and projections from the precision probes for the 125 GeV Higgs boson h were obtained in the previous section (Sec. III). Whereas, the current constraints are considered in the next section (Sec. V) along with some future projections for $(\delta, \kappa_{\text{inv}})$ from the direct searches for the exotic Higgs boson δ with $m_h/2 \leq m_\phi \leq 2m_h$ (for simplicity and easy compatibility with precision electroweak constraints). And, we will see that the precision probes for the observed Higgs boson h are typically much more constraining than the direct searches for the exotic Higgs ϕ .

V. CONSTRAINTS ON REAL SINGLET SCALARS

As mentioned above, in the present case the sine-squared of the mixing angle between the gauge eigenstates h_{SM} and S gives rise to the universal depletion factor δ for the couplings of the physical 125 GeV Higgs boson h , and the invisible width Γ_{inv} of S gives rise to the invisible width of h . Therefore, all of the constraints on $(\delta, \kappa_{\text{inv}})$ from the precision probes for the 125 GeV Higgs boson, considered in Sec. II, are directly applicable for $(\delta, \kappa_{\text{inv}})$ in the case of real scalar singlet extension to the SM.

Apart from the indirect constraints that come from the precision probes for the 125 GeV Higgs boson, there are also additional bounds on the exotic Higgs ϕ for various values of its mass m_ϕ from precision electroweak observables, and also from the collider searches for an additional neutral Higgs boson over a wide range of masses.

First, let us consider the bounds from precision electroweak observables, in particular from the Peskin-Takeuchi

parameters S , T , and U [47]. To that end we begin by noting the one-loop contribution of the SM Higgs with mass m to the massive vector boson ($V = W, Z$) propagators:

$$\Pi_{VV}(p^2; m) = -\frac{\alpha_e m_V^2}{4\pi s_W^2 m_W^2} \left[\frac{1}{2} A_0(m) + m_V^2 B_0(p^2; m_V, m) - B_{00}(p^2; m_V, m) \right], \quad (5.1)$$

where α_e is the fine structure constant, s_W (c_W) is the sine (cosine) of the weak-mixing angle, and $A_0(m_0)$, $B_0(p^2; m_1, m_0)$, and $B_{00}(p^2; m_1, m_0)$ are the Passarino-Veltman functions following the conventions of Ref. [48]. Then the predictions for the Peskin-Takeuchi parameters in the real singlet scalar extension to the SM are given by

$$S = \frac{4c_W^2 s_W^2}{\alpha_e} \left[\frac{\Pi_{ZZ}^{\text{new}}(m_Z^2) - \Pi_{ZZ}^{\text{new}}(0)}{m_Z^2} \right], \quad (5.2)$$

$$T = \frac{1}{\alpha_e} \left[\frac{\Pi_{WW}^{\text{new}}(0)}{m_W^2} - \frac{\Pi_{ZZ}^{\text{new}}(0)}{m_Z^2} \right], \quad (5.3)$$

$$U = \frac{4s_W^2}{\alpha_e} \left[\frac{\Pi_{WW}^{\text{new}}(m_W^2) - \Pi_{WW}^{\text{new}}(0)}{m_W^2} \right] - S, \quad (5.4)$$

with

$$\Pi_{VV}^{\text{new}}(p^2) = (1 - \delta^2) \Pi_{VV}(p^2; m_h) + \delta^2 \Pi_{VV}(p^2; m_\phi) - \Pi_{VV}(p^2; m_h), \quad (5.5)$$

such that the parameters S , T , and U account for the contribution of the physical Higgs boson with mass m_h that is already included in them, and therefore are normalized to reflect only the new physics (i.e., real scalar singlet Higgs) contribution.

From the global electroweak fit at NNLO by the Gfitter group [49], the current experimental measurements of the Peskin-Takeuchi parameters, with the SM reference point taken to be $(m_h, m_t) = (125, 173)$ GeV, are

$$\hat{S} = 0.05, \quad \hat{T} = 0.09, \quad \hat{U} = 0.01, \quad (5.6)$$

with the corresponding uncertainties (σ_i)

$$\sigma_S = 0.11, \quad \sigma_T = 0.13, \quad \sigma_U = 0.11, \quad (5.7)$$

and the correlation coefficients ($\rho_{ij} = \rho_{ji} = \frac{\sigma_{ij}}{\sigma_i \sigma_j}$)

$$\rho_{ST} = 0.90, \quad \rho_{SU} = -0.59, \quad \rho_{TU} = -0.83. \quad (5.8)$$

In order to finally obtain a bound on δ , we check the compatibility of the model predictions with that of the

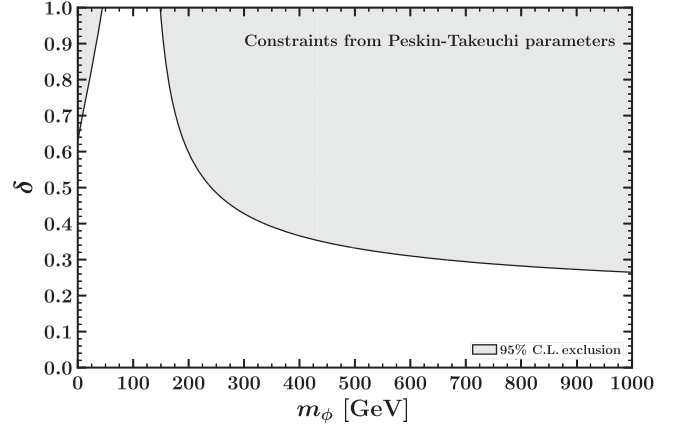


FIG. 2. Constraints on δ as a function of the exotic Higgs mass m_ϕ from precision electroweak observables S , T , and U parameters. The bounds are extracted by evaluating the χ^2 using the model predictions and observed values of Peskin-Takeuchi parameters, taking all the experimental uncertainties and correlations into account, and demanding that the resulting χ^2 corresponds to a 95% confidence level fit.

experimental measurements. In particular, for a chosen m_ϕ , we compute the χ^2 value, which is a function of δ , using

$$\chi^2 = \mathbf{y}_i \mathbf{V}_{ij}^{-1} \mathbf{y}_j, \quad (5.9)$$

with $\mathbf{y}_i = (S - \hat{S}, T - \hat{T}, U - \hat{U})$, and the covariance matrix elements $\mathbf{V}_{ii} = \sigma_i^2$ and $\mathbf{V}_{ij} = \rho_{ij} \sigma_i \sigma_j$ ($i \neq j$). And, solve for δ after requiring $\chi^2 = 7.81$ corresponding to a fit with 95% confidence level (or a p value of 0.05) with 3 degrees of freedom [26].

Figure 2 shows the bound obtained from Peskin-Takeuchi parameters using the procedure detailed above on δ as a function of m_ϕ . Actually, for a fixed significance level, we find a disagreement in comparing our results with the ones obtained in Refs. [16,17]. The reason for this disagreement is due to an additional factor of -1 that is included in the vacuum polarization function Π_{VV} which can be inferred from Eqs. (24) and (25) of Ref. [15],⁴ which seemed to have propagated into the results in Refs. [16,17]. Taking $\Pi_{VV} \rightarrow -\Pi_{VV}$ in Eq. (5.1), we exactly reproduce the bounds from S , T , and U parameters reported in Refs. [16,17]. To check the correctness of the sign in Eq. (5.1), we have computed the one-loop contribution of the SM Higgs to s_W^2 and checked that it agrees with the results in the standard quantum field theory textbooks, e.g., Refs. [50,51]. Furthermore, the constraints we obtain from S , T , and U parameters are in good agreement with that of Ref. [22], which uses the

⁴Additionally, in Eqs. (24) and (25) of Ref. [15], we note that there is an additional factor of $\frac{1}{2}$ in the term with $A_0(m)$, but that term drops out of the Peskin-Takeuchi parameters as it is independent of p^2 .

experimental inputs from Ref. [26]. We note that our results do not change significantly if we use experimental inputs from Ref. [26] instead of Ref. [49]. Therefore, in contrast to the claim in Refs. [16,17], S , T , and U electroweak precision parameters pose significant constraints on δ as a function of m_ϕ , especially for large m_ϕ .

We now turn to constraints on our parameter space from the collider searches for additional neutral Higgs boson. Once again, for invisible searches, an upper bound is given on μ_{inv} [defined in Eq. (3.1)], which translates into

$$\mu_{\text{inv}} = \frac{\delta^2(1 - \delta^2)\kappa_{\text{inv}}}{\kappa_{\text{inv}} + (\kappa_{\text{SM}} - \kappa_{\text{inv}})\delta^2}, \quad (5.10)$$

for the exotic Higgs ϕ . For a bound reported on μ_{inv} at each m_ϕ and for a fixed κ_{inv} , we can then solve for the allowed values of δ using the above equation.

For searches for additional Higgs boson in the j th SM final state, an upper limit is reported on

$$\mu = \frac{\sigma B_j}{\sigma_{\text{SM}} B_{\text{SM},j}}. \quad (5.11)$$

For the ϕ boson, this limit can be recasted, using Eq. (4.21), as

$$\mu = \frac{\delta^4 \kappa_{\text{SM}}}{\kappa_{\text{inv}} + (\kappa_{\text{SM}} - \kappa_{\text{inv}})\delta^2}, \quad (5.12)$$

from which we can extract the allowed values of δ for a fixed κ_{inv} for each m_ϕ . Various collider searches that look for (additional) neutral Higgs boson(s) in various decay channels (including invisible searches) that pose significant constraints on the parameter space of $(\delta, \kappa_{\text{inv}}, m_\phi)$ are listed in Table III. The relevant data associated with these searches was obtained, in part, from the files provided with the publicly available FORTRAN code HiggsBounds5 [52]. And

the widths and branching ratios of the SM Higgs boson for various masses are obtained using the program HDECAY [53,54].

In Fig. 3 we show various constraints on δ as a function of the exotic Higgs mass m_ϕ for various choices of κ_{inv} at 95% C.L. The shaded regions with solid borders are the bounds from the searches for the exotic Higgs ϕ decaying to SM final states, and the shaded regions with dashed borders are the bounds from the invisible searches for ϕ . The labels for each of these shaded regions correspond to the ones listed in Table III. Gold dashed lines show the constraints from electroweak precision observables, namely, the Peskin-Takeuchi S , T , and U parameters. And, dotted lines show the bounds from the precision probes for $h \rightarrow WW \rightarrow e\nu\mu\nu$ and $h \rightarrow \gamma\gamma$, which typically are much more constraining than the searches for ϕ . The 3D plots in Fig. 4 show the richness of various bounds from the searches for neutral Higgs bosons in various decay channels on the parameter space of $(\delta, \kappa_{\text{inv}}, m_\phi)$. Various 2D slices of the 3D plots in Fig. 4 with fixed κ_{inv} were shown in Fig. 3.

In Fig. 5, we show some future projections for δ as a function of the real singlet scalar mass m_ϕ for $\kappa_{\text{inv}} = 0, 1$. Here we only show the sensitivities of ILC for ϕ from the $\phi \rightarrow b\bar{b}$ decays and using a model-independent recoil mass method in the $e^+e^- \rightarrow Z\phi$ process [66–68]. The solid and dotted lines show the present collider constraints from the searches for ϕ and precision probes for h , respectively (see Figs. 1 and 3). The violet dashed lines show the projected sensitivity of the ILC with $\sqrt{s} = 250$ GeV for $\phi \rightarrow b\bar{b}$ searches [66] with 0.5 ab^{-1} and beam polarization of (80,30)% for (e^-, e^+) , respectively. The orange dashed lines show the expected sensitivity, obtained using the model-independent recoil mass method in the $e^+e^- \rightarrow Z\phi$ process, of the 250 GeV ILC with integrated luminosity of $(0.9, 0.9, 0.1, 0.1) \text{ ab}^{-1}$ for $(e_L^- e_R^+, e_R^- e_L^+, e_L^- e_L^+, e_R^- e_R^+)$, respectively, and beam polarization of (80, 30)% for

TABLE III. Collider searches for the decays of (additional) neutral Higgs boson(s) to (visible) SM and invisible final states over wide range of masses. For convenience, various searches are assigned labels which will be used in the figures below. $B_{\text{SM},j}$ below is the SM branching ratio for $h_{\text{SM}} \rightarrow j$ th SM final state.

Label	Mass range (GeV)	Limit reported (95% C.L.)	References
LEP 2005 ($\phi \rightarrow \text{inv}$)	50–110	μ_{inv}	[55]
LEP 2011 ($\phi \rightarrow \text{inv}$)	90–118	μ_{inv}	[56]
CMS 2018 ($\phi \rightarrow \text{inv}$)	110–1000	μ_{inv}	[25]
ATLAS 2019 ($\phi \rightarrow \text{inv}$)	75–3000	$\mu_{\text{inv}}\sigma_{\text{SM}}$	[57]
ATLAS 2022 ($\phi \rightarrow \text{inv}$)	50–2000	$\mu_{\text{inv}}\sigma_{\text{SM}}$	[58]
LEP 2006 ($\phi \rightarrow b\bar{b}$)	12–120	$\mu B_{\text{SM},b\bar{b}}$	[59]
CMS 2012 (combined)	110–1000	μ	[60]
CMS 2013 ($\phi \rightarrow WW$)	110–600	μ	[61]
CMS 2015 ($\phi \rightarrow WW/ZZ$)	145–1000	μ	[62]
ATLAS 2015 ($\phi \rightarrow ZZ$)	140–1000	$\mu\sigma_{\text{SM}}B_{\text{SM},ZZ}$	[63]
ATLAS 2020 ($\phi \rightarrow ZZ$)	210–2000	$\mu\sigma_{\text{SM}}B_{\text{SM},ZZ}$	[64]
CMS 2018 ($\phi \rightarrow ZZ$)	130–3000	$\mu\sigma_{\text{SM}}B_{\text{SM},ZZ}$	[65]

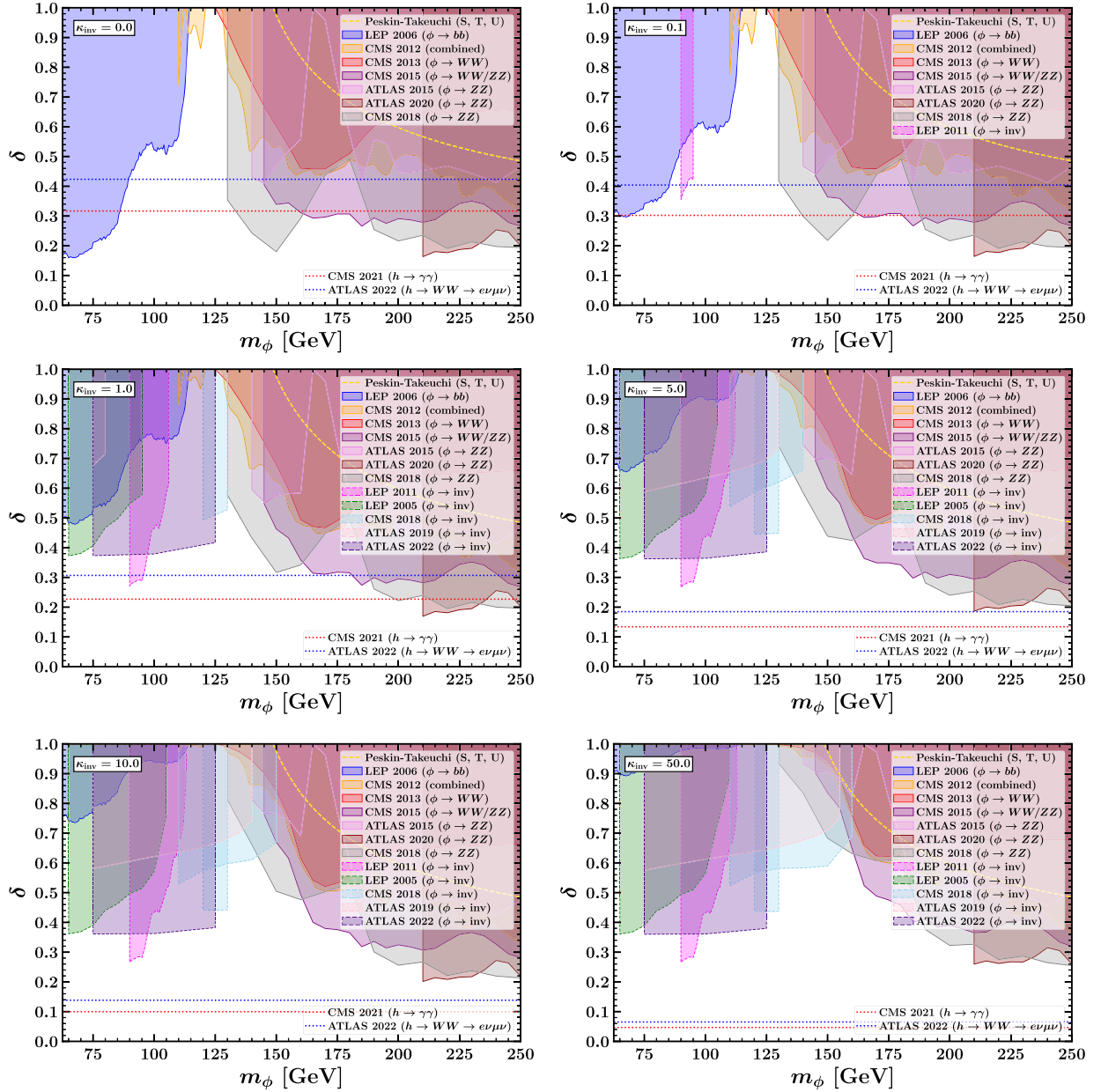


FIG. 3. 95% C.L. bounds on δ as a function of the exotic Higgs mass m_ϕ for various choices of $\kappa_{\text{inv}} = 0, 0.1, 1, 5, 10, 50$. The shaded regions with solid borders are the bounds from the searches for $\phi \rightarrow$ (visible) SM final states, and the shaded regions with dashed borders are the bounds from the invisible searches for ϕ . The labels for each of these shaded regions correspond to the ones listed in Table III. Gold dashed lines show the constraints from electroweak precision observables, namely, the Peskin-Takeuchi $S, T,$ and U parameters. The dotted lines show the indirect constraints from the precision probes for $h \rightarrow WW \rightarrow e\nu\mu\nu$ and $h \rightarrow \gamma\gamma$ (strongest bound in most cases).

(e^-, e^+), respectively [67]. And, the green dashed lines show similar results but with 500 GeV ILC with integrated luminosity of (1.6, 1.6, 0.4, 0.4) ab^{-1} for ($e_L^- e_L^+, e_R^- e_R^+, e_L^- e_L^+, e_R^- e_R^+$), respectively [67]. Both the orange and green dashed lines are independent of the choice for κ_{inv} as the mass of ϕ can be measured using the recoil mass against the Z boson (reconstructed from $\mu^+\mu^-$) independent of the decays of ϕ . The dash-dotted lines in the right panel with $\kappa_{\text{inv}} = 1$ are the future projections for invisible searches of

the observed Higgs boson h at HL-LHC and 250 GeV ILC (see Fig. 1) that indirectly constrain the parameter space.

To summarize, we recasted the bounds/projections reported in various collider searches/studies, for neutral Higgs boson(s), for the depletion factors ($\delta, \kappa_{\text{inv}}$) of the already discovered 125 GeV Higgs boson h that occur in the SM extended with a real scalar singlet. And, we found that the precision studies of the observed Higgs boson h often provide for the strongest constraint/reach in the parameter

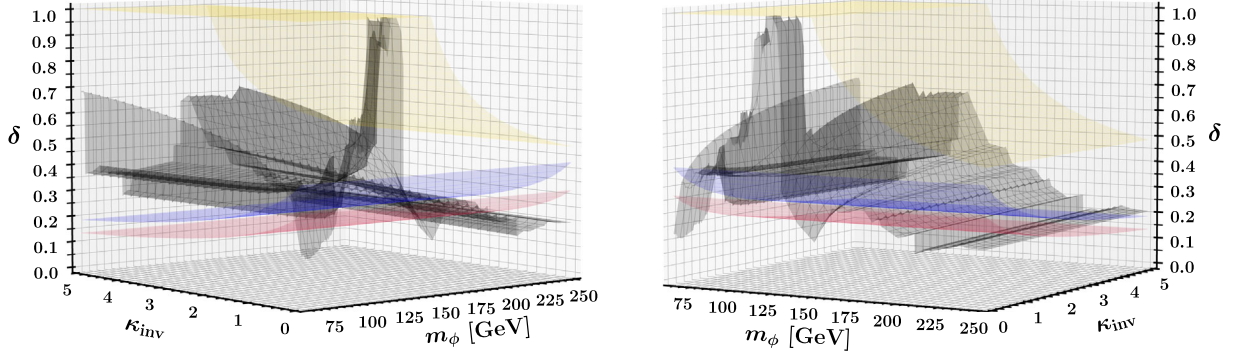


FIG. 4. Constraints on the 3D parameter space $(\delta, \kappa_{\text{inv}}, m_\phi)$ from the collider searches for ϕ (black shaded envelope; listed in Table III), along with the strongest constraints from the precision probes for $h \rightarrow \gamma\gamma$ (red) and $h \rightarrow WW \rightarrow e\nu\mu\nu$ (blue). Also shown are the constraints from the Peskin-Takeuchi parameters for the SM extended with a real SM gauge-singlet scalar Higgs (gold). The 3D plots here showcase various bounds on all the free parameters of this model, and more details are shown in Fig. 3 with some 2D slices with fixed κ_{inv} .

space $(\delta, \kappa_{\text{inv}}, m_\phi)$ compared to the direct searches for the additional physical Higgs ϕ , at least for $m_h/2 \leq m_\phi \leq 2m_h$. For large m_ϕ , we found that the precision electroweak observables S , T , and U can impose a strong constraint on the parameter space. The results obtained in this section for the real singlet scalar extension suggest that in various other extended Higgs sectors that contain the depleted Higgs boson, the precision probes for the 125 GeV Higgs boson alone can often best constrain such a class of models.

VI. HIGH MULTIPLICITY OF REAL SINGLET SCALARS

Finally, we also briefly consider an extension to the SM with N real SM gauge-singlet scalars $S_{i=1,2,\dots,N}$, each with

an invisible width Γ_{inv} , where the gauge basis $\{h_{\text{SM}}, S_i\}$ is related to the mass basis $\{h, \phi_i\}$ in the following way:

$$\begin{pmatrix} h_{\text{SM}} \\ S_1 \\ S_2 \\ \vdots \\ \vdots \end{pmatrix} = \begin{pmatrix} \sqrt{1-\delta^2} & \eta & \eta & \dots \\ -\eta & 1+\epsilon & \epsilon & \dots \\ -\eta & \epsilon & 1+\epsilon & \dots \\ \vdots & \vdots & \vdots & \dots \\ \vdots & \vdots & \vdots & \dots \end{pmatrix} \begin{pmatrix} h \\ \phi_1 \\ \phi_2 \\ \vdots \\ \vdots \end{pmatrix}. \quad (6.1)$$

Here, for purposes of illustration, we chose that the gauge-singlets S_i mix equally among themselves (parametrized by ϵ) and with the SM Higgs h_{SM} (parametrized by η). Note that h here stands for the physical Higgs boson with mass ~ 125 GeV that is already discovered, and ϕ_i are the exotic

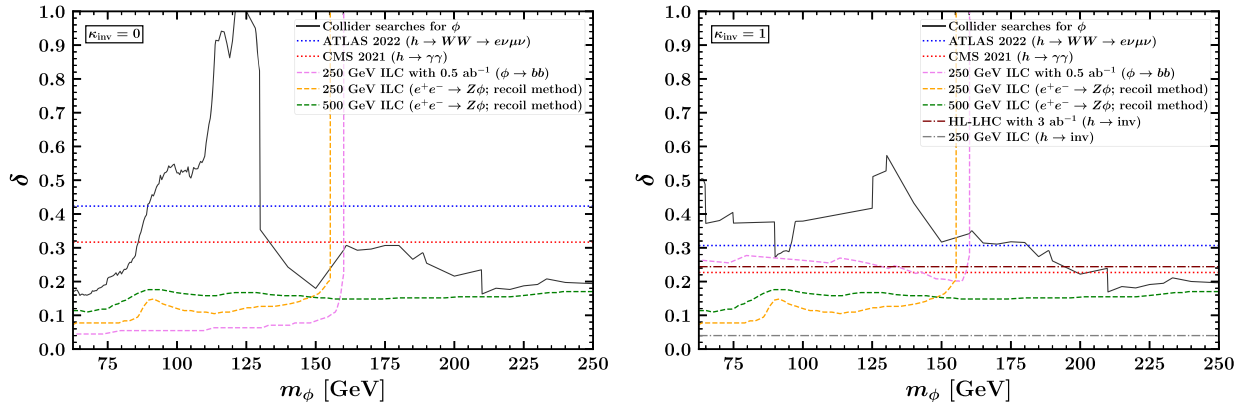


FIG. 5. Some future sensitivities for δ as a function of the real singlet scalar mass m_ϕ for $\kappa_{\text{inv}} = 0$ (left panel) and $\kappa_{\text{inv}} = 1$ (right panel). The solid and dotted lines show the present collider constraints from the searches for ϕ and precision probes for h , respectively (see Figs. 1 and 3). The violet dashed lines show the projected sensitivity of the 250 GeV ILC for $\phi \rightarrow b\bar{b}$ searches with some modest running assumptions [66] as discussed in the text. The (orange, green) dashed lines show the model-independent expected sensitivity at the ILC with $\sqrt{s} = (250, 500)$ GeV, respectively, with various running assumptions [67] as mentioned in the text. The (maroon, gray) dash-dotted lines in the right panel are future projections for invisible searches of the observed Higgs boson h from Fig. 1 at (HL-LHC with 3 ab^{-1} [40], 250 GeV ILC with 1.8 ab^{-1} [46]), respectively, that indirectly constrain the parameter space.

Higgs with masses taken to be $m_h/2 \leq m_{\phi_i} \leq 2m_h$ for simplicity. The orthogonality of the above matrix implies that

$$\eta = \frac{\delta}{\sqrt{N}}, \quad (6.2)$$

$$\epsilon = \frac{1}{N}(\sqrt{1-\delta^2} - 1) = -\frac{\delta^2}{2N} + \dots \quad (6.3)$$

The gauge eigenstates can be expressed in terms of the mass eigenstates:

$$h_{\text{SM}} = \sqrt{1-\delta^2}h + \frac{\delta}{\sqrt{N}} \sum_{i=1}^N \phi_i, \quad (6.4)$$

$$S_i = -\frac{\delta}{\sqrt{N}}h + \phi_i + \frac{1}{N}(\sqrt{1-\delta^2} - 1) \sum_{j=1}^N \phi_j. \quad (6.5)$$

We once again find that the total widths, branching ratios, and production cross sections of h are the same as in Sec. II, and for the exotic Higgs bosons ϕ_i , the results for ϕ from Sec. IV are directly applicable but with the replacement $\delta \rightarrow \eta = \frac{\delta}{\sqrt{N}}$, for example,

$$\frac{\Gamma^{\phi_i}}{\Gamma_{\text{SM}}} = \frac{\delta^2}{N} + \left(1 - \frac{\delta^2}{N}\right) \frac{\kappa_{\text{inv}}}{\kappa_{\text{SM}}}. \quad (6.6)$$

Therefore all the bounds in Sec. V can be reinterpreted for each ϕ_i by simply rescaling the bounds by \sqrt{N} . We can then immediately see that the bounds coming from the searches for ϕ_i become weaker as N gets larger, and the strongest constraints often come directly from the precision

probes for the 125 GeV Higgs boson h . To illustrate this, we randomly generate $m_{\phi_i} \in [m_h/2, 2m_h]$ and choose the strongest bound from the bounds obtained for each m_{ϕ_i} . We then iterate these steps several times, so that it is evident that the strongest bound always (often) comes from the precision probes for the 125 GeV Higgs boson h for large (small) N .

Figure 6 shows various bounds on δ as a function of number of SM gauge-singlet real scalars N for fixed κ_{inv} . Dotted lines show the constraints coming from the precision probes for the 125 GeV Higgs boson h , specifically the most stringent ones from the precision probes for $h \rightarrow \gamma\gamma$ by CMS and $h \rightarrow WW \rightarrow e\nu\mu\nu$ by ATLAS. The orange-colored square scatter plot shows the strongest bound on δ from searches for ϕ_i for all $m_{\phi_i} \in [m_h/2, m_h]$. For example, for $\kappa_{\text{inv}} = 0$, the strongest bound on η can be directly read off of the top-left plot of Fig. 3 to be ~ 0.16 at $m_{\phi_i} \sim 65$ GeV and so the strongest bound on $\delta = 0.16\sqrt{N}$. Various light-gray scatter plots are the strongest bounds obtained by randomly distributing all m_{ϕ_i} between 62.5 and 250 GeV. And, in Fig. 7, we show various bounds on δ as a function of κ_{inv} . Dotted lines, once again, show the bounds from the precision probes for the observed Higgs boson h . Thick solid lines show the strongest bounds from the searches for ϕ_i (for all m_{ϕ_i}) for real scalar singlet extensions with $N = 2$ and $N = 10$ scalars. Each thin solid line shows the strongest bounds obtained by randomly choosing m_{ϕ_i} in between $m_h/2$ and $2m_h$. As mentioned before, it is clear from Figs. 6 and 7 that the strongest bounds almost always come from the precision probes for the 125 GeV Higgs boson h for large N and/or large κ_{inv} .

Therefore, as remarked at the end of the previous section, we found that the indirect precision probes for the observed Higgs boson with $m_h \sim 125$ GeV tend to give the most

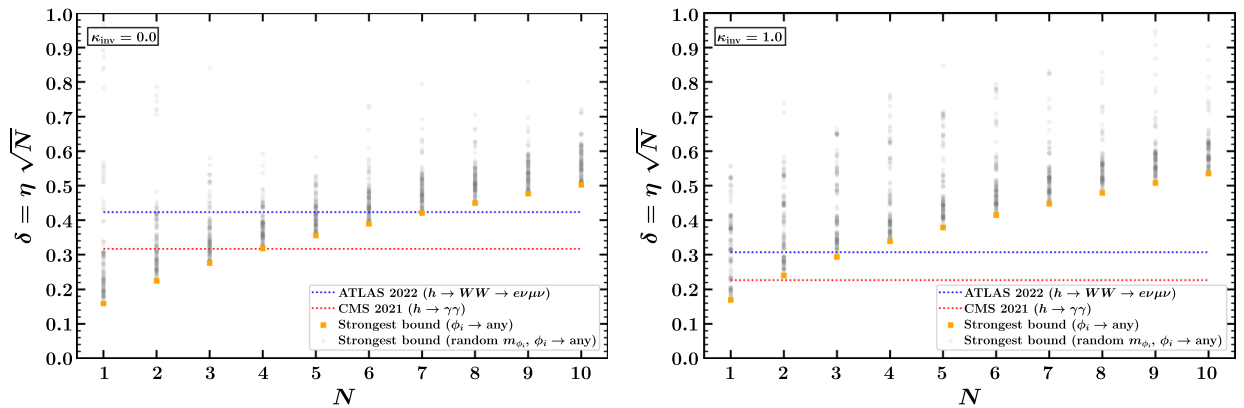


FIG. 6. Constraints on δ for the SM extended with N real singlet scalars for $\kappa_{\text{inv}} = 0$ (left panel) and $\kappa_{\text{inv}} = 1$ (right panel). Dotted lines show the strongest bounds from the precision probes for the 125 GeV Higgs h , scatter plot with square markers show the strongest bound from the searches for the exotic Higgs bosons ϕ_i obtained by varying the mass of one of the exotic Higgs m_{ϕ_i} from $m_h/2$ to $2m_h$. And the light-gray scatter plots show the strongest constraints in various iterations where the masses $m_{\phi_{i=1,\dots,N}}$ are randomly distributed between $m_h/2$ and $2m_h$, illustrating that the precision probes for the 125 GeV Higgs boson h alone typically provide for the strongest constraints.

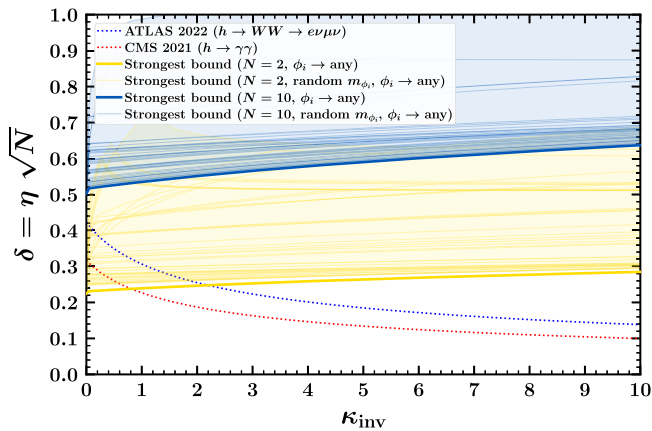


FIG. 7. Constraints on δ for the SM extended with N real singlet scalars as a function of κ_{inv} . The dotted lines show the strongest bounds from the (visible) precision probes for the 125 GeV Higgs h , and the thicker solid lines show the strongest bound from the searches for the exotic Higgs bosons ϕ_i obtained by varying the mass of one of the exotic Higgs m_{ϕ_i} from $m_h/2$ to $2m_h$ for $N = 2$ (blue) and $N = 10$ (yellow). And the thinner solid lines show the strongest constraints in various iterations where the masses $m_{\phi_{i=1,\dots,N}}$ are randomly distributed between $m_h/2$ and $2m_h$, illustrating that the precision probes for the 125 GeV Higgs boson h alone typically provide for the strongest constraints.

powerful constraint on the depletion factors $(\delta, \kappa_{\text{inv}})$ in the SM extended with a high multiplicity of real singlet scalars, albeit under some simplifying assumptions. And, the constraints from the direct searches for the additional exotic Higgs states ϕ_i get weaker as the multiplicity or the invisible width of the scalars increase.

VII. CONCLUSION

In this paper, we obtained the latest bounds on the universal depletion factor δ that suppresses all the couplings of the observed Higgs boson h to SM final states from the recent LHC searches in various decay channels as a function of the other depletion factor κ_{inv} , a parameter related to the invisible width of h [see Eq. (2.3)]. We argued that these bounds indirectly constrain many extended Higgs

sectors that give rise to δ and κ_{inv} , and are also in general comparable to or stronger than the direct searches for the additional Higgs states, at least if their masses are in between $m_h/2$ and $2m_h$.

To demonstrate we considered various bounds that come from the collider searches for an exotic Higgs boson ϕ that occurs in the SM extended with a real SM gauge-singlet scalar that decays only invisibly to some exotic hidden sector fermions. We also obtained the constraints on δ as a function of the mass of the exotic Higgs from precision electroweak observables (in particular the Peskin-Takeuchi parameters). Although, the constraints from the S , T , and U parameters are not the strongest bounds for $m_h/2 \leq m_\phi \leq 2m_h$, these bounds get very strong for higher m_ϕ . And, moreover, we also considered some future sensitivities for the observed Higgs boson h and for the exotic Higgs boson ϕ , to show that the parameter space of the extended Higgs sectors, that lead to the universal depletion factor δ and an invisible width factor κ_{inv} for h , get more constrained and will eventually measure the deviations from the SM predictions and lead the way to the discovery of the additional Higgs states.

Finally, we also considered the case where there are actually N real singlet scalars, with some simplifying assumptions for illustration purposes, and found that the indirect bounds from the precision probes for the 125 GeV Higgs boson h alone tend to moderately constrain such scenarios. The cases with larger number of such scalars and/or larger invisible widths for h are much more constrained from the indirect searches.

ACKNOWLEDGMENTS

We thank John Thiels for his help and support in using the Great Lakes cluster at University of Michigan. This research is supported in part through computational resources and services provided by Advanced Research Computing (ARC), a division of Information and Technology Services (ITS) at the University of Michigan, Ann Arbor. This work is supported in part by the Department of Energy under Grant No. DE-SC0007859.

- [1] T. Biekötter and M. Pierre, Higgs-boson visible and invisible constraints on hidden sectors, *Eur. Phys. J. C* **82**, 1026 (2022).
- [2] E. Fernández-Martínez, J. López-Pavón, J. M. No, T. Ota, and S. Rosauero-Alcaraz, ν electroweak baryogenesis: The scalar singlet strikes back, [arXiv:2210.16279](https://arxiv.org/abs/2210.16279).
- [3] J. D. Wells, Extra dimensions and the universal suppression of Higgs boson observables at high-energy colliders, [arXiv:hep-ph/0205328](https://arxiv.org/abs/hep-ph/0205328).

- [4] R. M. Schabinger and J. D. Wells, A minimal spontaneously broken hidden sector and its impact on Higgs boson physics at the large hadron collider, *Phys. Rev. D* **72**, 093007 (2005).
- [5] S. P. Martin and J. D. Wells, Motivation and detectability of an invisibly decaying Higgs boson at the Fermilab Tevatron, *Phys. Rev. D* **60**, 035006 (1999).
- [6] M. Bowen, Y. Cui, and J. D. Wells, Narrow trans-TeV Higgs bosons and $H \rightarrow hh$ decays: Two LHC search paths for a

- hidden sector Higgs boson, *J. High Energy Phys.* **03** (2007) 036.
- [7] J. McDonald, Gauge singlet scalars as cold dark matter, *Phys. Rev. D* **50**, 3637 (1994).
- [8] B. Patt and F. Wilczek, Higgs-field portal into hidden sectors, [arXiv:hep-ph/0605188](https://arxiv.org/abs/hep-ph/0605188).
- [9] D. O'Connell, M. J. Ramsey-Musolf, and M. B. Wise, Minimal extension of the Standard Model scalar sector, *Phys. Rev. D* **75**, 037701 (2007).
- [10] S. Profumo, M. J. Ramsey-Musolf, and G. Shaughnessy, Singlet Higgs phenomenology and the electroweak phase transition, *J. High Energy Phys.* **08** (2007) 010.
- [11] V. Barger, P. Langacker, M. McCaskey, M. J. Ramsey-Musolf, and G. Shaughnessy, LHC phenomenology of an extended Standard Model with a real scalar singlet, *Phys. Rev. D* **77**, 035005 (2008).
- [12] D. Bertolini and M. McCullough, The social Higgs, *J. High Energy Phys.* **12** (2012) 118.
- [13] J. R. Espinosa, T. Konstandin, and F. Riva, Strong electroweak phase transitions in the Standard Model with a singlet, *Nucl. Phys.* **B854**, 592 (2012).
- [14] G. M. Pruna and T. Robens, Higgs singlet extension parameter space in the light of the LHC discovery, *Phys. Rev. D* **88**, 115012 (2013).
- [15] D. López-Val and T. Robens, Δr and the W-boson mass in the singlet extension of the Standard Model, *Phys. Rev. D* **90**, 114018 (2014).
- [16] T. Robens and T. Stefaniak, Status of the Higgs singlet extension of the standard model after LHC run 1, *Eur. Phys. J. C* **75**, 104 (2015).
- [17] T. Robens and T. Stefaniak, LHC benchmark scenarios for the real Higgs singlet extension of the standard model, *Eur. Phys. J. C* **76**, 268 (2016).
- [18] A. Ilnicka, T. Robens, and T. Stefaniak, Constraining extended scalar sectors at the LHC and beyond, *Mod. Phys. Lett. A* **33**, 1830007 (2018).
- [19] S. Dawson and W. Yan, Hiding the Higgs boson with multiple scalars, *Phys. Rev. D* **79**, 095002 (2009).
- [20] C. Y. Chen, S. Dawson, and I. M. Lewis, Exploring resonant di-Higgs boson production in the Higgs singlet model, *Phys. Rev. D* **91**, 035015 (2015).
- [21] S. Dawson and I. M. Lewis, NLO corrections to double Higgs boson production in the Higgs singlet model, *Phys. Rev. D* **92**, 094023 (2015).
- [22] S. Dawson, P. P. Giardino, and S. Homiller, Uncovering the high scale Higgs singlet model, *Phys. Rev. D* **103**, 075016 (2021).
- [23] A. Falkowski, C. Gross, and O. Lebedev, A second Higgs from the Higgs portal, *J. High Energy Phys.* **05** (2015) 057.
- [24] ATLAS Collaboration, Combination of searches for invisible Higgs boson decays with the ATLAS experiment, Report No. ATLAS-CONF-2020-052.
- [25] A. M. Sirunyan *et al.* (CMS Collaboration), Search for invisible decays of a Higgs boson produced through vector boson fusion in proton-proton collisions at $\sqrt{s} = 13$ TeV, *Phys. Lett. B* **793**, 520 (2019).
- [26] P. A. Zyla *et al.* (Particle Data Group), Review of particle physics, *Prog. Theor. Exp. Phys.* **2020**, 083C01 (2020).
- [27] A. M. Sirunyan *et al.* (CMS Collaboration), Measurements of Higgs boson production cross sections and couplings in the diphoton decay channel at $\sqrt{s} = 13$ TeV, *J. High Energy Phys.* **07** (2021) 027.
- [28] ATLAS Collaboration, Measurement of the properties of Higgs boson production at $\sqrt{s} = 13$ TeV in the $H \rightarrow \gamma\gamma$ channel using 139 fb^{-1} of pp collision data with the ATLAS experiment, [arXiv:2207.00348](https://arxiv.org/abs/2207.00348).
- [29] G. Aad *et al.* (ATLAS Collaboration), Higgs boson production cross-section measurements and their EFT interpretation in the 4ℓ decay channel at $\sqrt{s} = 13$ TeV with the ATLAS detector, *Eur. Phys. J. C* **80**, 957 (2020); **81**, 29(E) (2021); **81**, 398(E) (2021).
- [30] A. M. Sirunyan *et al.* (CMS Collaboration), Measurements of production cross sections of the Higgs boson in the four-lepton final state in proton-proton collisions at $\sqrt{s} = 13$ TeV, *Eur. Phys. J. C* **81**, 488 (2021).
- [31] ATLAS Collaboration, Measurements of Higgs boson production by gluon-gluon fusion and vector-boson fusion using $H \rightarrow WW^* \rightarrow e\nu\mu\nu$ decays in pp collisions at $\sqrt{s} = 13$ TeV with the ATLAS detector, [arXiv:2207.00338](https://arxiv.org/abs/2207.00338).
- [32] A. M. Sirunyan *et al.* (CMS Collaboration), Measurement of the inclusive and differential Higgs boson production cross sections in the leptonic WW decay mode at $\sqrt{s} = 13$ TeV, *J. High Energy Phys.* **03** (2021) 003.
- [33] A. M. Sirunyan *et al.* (CMS Collaboration), Observation of Higgs Boson Decay to Bottom Quarks, *Phys. Rev. Lett.* **121**, 121801 (2018).
- [34] M. Aaboud *et al.* (ATLAS Collaboration), Observation of $H \rightarrow b\bar{b}$ decays and VH production with the ATLAS detector, *Phys. Lett. B* **786**, 59 (2018).
- [35] G. Aad *et al.* (ATLAS Collaboration), Measurements of Higgs boson production cross-sections in the $H \rightarrow \tau^+\tau^-$ decay channel in pp collisions at $\sqrt{s} = 13$ TeV with the ATLAS detector, *J. High Energy Phys.* **08** (2022) 175.
- [36] CMS Collaboration, Measurements of Higgs boson production in the decay channel with a pair of τ leptons in proton-proton collisions at $\sqrt{s} = 13$ TeV, [arXiv:2204.12957](https://arxiv.org/abs/2204.12957).
- [37] A. M. Sirunyan *et al.* (CMS Collaboration), Evidence for Higgs boson decay to a pair of muons, *J. High Energy Phys.* **01** (2021) 148.
- [38] G. Aad *et al.* (ATLAS Collaboration), A search for the dimuon decay of the Standard Model Higgs boson with the ATLAS detector, *Phys. Lett. B* **812**, 135980 (2021).
- [39] K. Fujii, C. Grojean, M. E. Peskin, T. Barklow, Y. Gao, S. Kanemura, H. D. Kim, J. List, M. Nojiri, M. Perelstein *et al.*, Physics case for the international linear collider, [arXiv:1506.05992](https://arxiv.org/abs/1506.05992).
- [40] Z. Liu, L. T. Wang, and H. Zhang, Exotic decays of the 125 GeV Higgs boson at future e^+e^- lepton colliders, *Chin. Phys. C* **41**, 063102 (2017).
- [41] J. de Blas, M. Cepeda, J. D'Hondt, R. K. Ellis, C. Grojean, B. Heinemann, F. Maltoni, A. Nisati, E. Petit, R. Rattazzi *et al.*, Higgs boson studies at future particle colliders, *J. High Energy Phys.* **01** (2020) 139.
- [42] A. Ayshev *et al.*, The international linear collider: Report to Snowmass 2021, [arXiv:2203.07622](https://arxiv.org/abs/2203.07622).
- [43] G. Bernardi, E. Brost, D. Denisov, G. Landsberg, M. Aleksa, D. d'Enterria, P. Janot, M. L. Mangano, M. Selvaggi, F. Zimmermann *et al.*, The future circular collider:

- A summary for the US 2021 Snowmass process, [arXiv:2203.06520](https://arxiv.org/abs/2203.06520).
- [44] J. de Blas, J. Gu, and Z. Liu, Higgs precision at a 125 GeV muon collider, *Phys. Rev. D* **106**, 073007 (2022).
- [45] M. Forslund and P. Meade, High precision Higgs from high energy muon colliders, *J. High Energy Phys.* **08** (2022) 185.
- [46] C. Potter, A. Steinhebel, J. Brau, A. Pryor, and A. White, Expected sensitivity to invisible Higgs boson decays at the ILC with the SiD detector (A Snowmass White Paper), [arXiv:2203.08330](https://arxiv.org/abs/2203.08330).
- [47] M. E. Peskin and T. Takeuchi, Estimation of oblique electroweak corrections, *Phys. Rev. D* **46**, 381 (1992).
- [48] H. H. Patel, Package-X: A *Mathematica* package for the analytic calculation of one-loop integrals, *Comput. Phys. Commun.* **197**, 276 (2015).
- [49] M. Baak, J. Cúth, J. Haller, A. Hoecker, R. Kogler, K. Mönig, M. Schott, and J. Stelzer (Gfitter Group), The global electroweak fit at NNLO and prospects for the LHC and ILC, *Eur. Phys. J. C* **74**, 3046 (2014).
- [50] M. E. Peskin and D. V. Schroeder, *An Introduction to Quantum Field Theory* (Westview Press, Reading, USA, 1995).
- [51] M. D. Schwartz, *Quantum Field Theory and the Standard Model* (Cambridge University Press, Cambridge, England, 2014).
- [52] P. Bechtle, D. Dercks, S. Heinemeyer, T. Klingl, T. Stefaniak, G. Weiglein, and J. Wittbrodt, HiggsBounds-5: Testing Higgs sectors in the LHC 13 TeV Era, *Eur. Phys. J. C* **80**, 1211 (2020).
- [53] A. Djouadi, J. Kalinowski, M. Muehlleitner, and M. Spira, HDECAY: Twenty₊₊ years after, *Comput. Phys. Commun.* **238**, 214 (2019).
- [54] A. Djouadi, J. Kalinowski, and M. Spira, HDECAY: A program for Higgs boson decays in the Standard Model and its supersymmetric extension, *Comput. Phys. Commun.* **108**, 56 (1998).
- [55] P. Achard *et al.* (L3 Collaboration), Search for an invisibly-decaying Higgs boson at LEP, *Phys. Lett. B* **609**, 35 (2005).
- [56] LEP Higgs Working for Higgs boson searches, ALEPH, DELPHI, L3 CERN, and OPAL Collaborations, Searches for invisible Higgs bosons: Preliminary combined results using LEP data collected at energies up to 209-GeV, [arXiv:hep-ex/0107032](https://arxiv.org/abs/hep-ex/0107032).
- [57] M. Aaboud *et al.* (ATLAS Collaboration), Search for invisible Higgs boson decays in vector boson fusion at $\sqrt{s} = 13$ TeV with the ATLAS detector, *Phys. Lett. B* **793**, 499 (2019).
- [58] G. Aad *et al.* (ATLAS Collaboration), Search for invisible Higgs-boson decays in events with vector-boson fusion signatures using 139 fb⁻¹ of proton-proton data recorded by the ATLAS experiment, *J. High Energy Phys.* **08** (2022) 104.
- [59] S. Schael *et al.* (ALEPH, DELPHI, L3, OPAL, and LEP Working Group for Higgs Boson Searches Collaborations), Search for neutral MSSM Higgs bosons at LEP, *Eur. Phys. J. C* **47**, 547 (2006).
- [60] CMS Collaboration, Combination of standard model Higgs boson searches and measurements of the properties of the new boson with a mass near 125 GeV, Report No. CMS-PAS-HIG-12-045.
- [61] CMS Collaboration, Update on the search for the standard model Higgs boson in pp collisions at the LHC decaying to $W + W$ in the fully leptonic final state, Report No. CMS-PAS-HIG-13-003.
- [62] V. Khachatryan *et al.* (CMS Collaboration), Search for a Higgs boson in the mass range from 145 to 1000 GeV decaying to a pair of W or Z bosons, *J. High Energy Phys.* **10** (2015) 144.
- [63] G. Aad *et al.* (ATLAS Collaboration), Search for an additional, heavy Higgs boson in the $H \rightarrow ZZ$ decay channel at $\sqrt{s} = 8$ TeV in pp collision data with the ATLAS detector, *Eur. Phys. J. C* **76**, 45 (2016).
- [64] G. Aad *et al.* (ATLAS Collaboration), Search for heavy resonances decaying into a pair of Z bosons in the $\ell^+\ell^-\ell'^+\ell'^-$ and $\ell^+\ell^-\nu\bar{\nu}$ final states using 139 fb⁻¹ of proton-proton collisions at $\sqrt{s} = 13$ TeV with the ATLAS detector, *Eur. Phys. J. C* **81**, 332 (2021).
- [65] A. M. Sirunyan *et al.* (CMS Collaboration), Search for a new scalar resonance decaying to a pair of Z bosons in proton-proton collisions at $\sqrt{s} = 13$ TeV, *J. High Energy Phys.* **06** (2018) 127; **03** (2019) 128(E).
- [66] P. Drechsel, G. Moortgat-Pick, and G. Weiglein, Prospects for direct searches for light Higgs bosons at the ILC with 250 GeV, *Eur. Phys. J. C* **80**, 922 (2020).
- [67] Y. Wang, M. Berggren, and J. List, ILD benchmark: Search for extra scalars produced in association with a Z boson at $\sqrt{s} = 500$ GeV, [arXiv:2005.06265](https://arxiv.org/abs/2005.06265).
- [68] T. Robens, A short overview on low mass scalars at future lepton colliders—Snowmass White Paper, [arXiv:2203.08210](https://arxiv.org/abs/2203.08210).